# Crustal Softening at Propagating Rift Tips, East Africa

F. Kolawole[1,2], R. Ajala[1]

[1]Lamont-Doherty Earth Observatory of Columbia University, Palisades, New York, 10964, United States
[2]Department of Earth and Environmental Sciences, Columbia University, New York, 10027, United States

*Correspondence to*: Folarin Kolawole (fola@ldeo.columbia.edu)

**Abstract**

We investigate the upper-crustal structure of the Rukwa-Tanganyika Rift Zone, East Africa, where earthquakes anomalously cluster at the northwestern tip of the Rukwa Rift, the eastern tip of the Mweru-Wantipa Rift, and along the Tanganyika Rift axis. The current rift tips host distributed faulting in exposed basement with little sedimentation. Here, we invert earthquake P and S travel times to produce three-dimensional upper-crustal velocity models for the region. The resulting models reveal the occurrence of anomalously high Vp/Vs ratios that extend from the surface down to ca. 10 km at the tip zones of the Rukwa and Mweru-Wantipa rifts. The spatial association of distributed faulting, upper-crustal seismicity, and thermal anomalies with the high Vp/Vs ratios suggest a weakened crust below the rift tips' flexural zone. We propose an ongoing strain localization and crustal softening at the rift tips that is accommodated by brittle damage from bending strain, and potentially compounded by hydrothermal weakening. This setting represents a precursory phase that may initiate unilateral rift tip propagation.

## 1 Introduction

The mechanism of segmentation and lateral propagation and linkage of continental rifts, first introduced by Bosworth (1985), has received significant attention from the scientific community as they influence the structure and temporal progression of the evolving break-up axis (e.g., Ebinger et al., 1989, 1999; Nelson et al., 1992; Acocella, 1999; Aanyu and Koehn, 2011; Allken et al., 2012; Corti, 2004; Zwaan et al., 2016; Neuharth et al., 2021; Kolawole et al., 2021a; Brune et al., 2023). Previous studies have established that continental rift systems grow by initial nucleation of isolated segments that propagate laterally, interact, link up, and coalesce to form longer composite rift basins with a continuous rift floor. Prior to linkage, the propagating rift segments are separated by an 'unrifted' basement block, and the lateral propagation of the rift deformation into the intervening block is essential to advance the rift system towards break-up (e.g., Nelson et al., 1992; Kolawole et al., 2021a; Brune et al., 2023).

In regions of active tectonic extension, inelastic deformation manifests by tectonic and magmatic deformation of the crystalline crust and its overlying sedimentary sequences in the rift basins (e.g., Brune et al., 2023; Pérez-Gussinyé et al., 2023). However, in magma-poor (i.e., non-volcanic) active rift settings, tectonic deformation in continental rifts is commonly accommodated by widespread brittle deformation of the crust through faulting and fracturing and accompanied by earthquakes (e.g., Muirhead et al., 2019; Kolawole et al., 2017, 2018; Gaherty et al., 2019; Zheng et al., 2020; Stevens et al., 2021). Nevertheless, little is

known of how this deformation is transferred onto the propagating rift tips, and long-standing questions remain on how the earth's crystalline crust accommodates and localizes tectonic strain during continental rift propagation.

Here, we utilize recently acquired seismic data to explore the upper crustal structure of the Rukwa-Tanganyika Rift Zone (Fig. 1a), an active non-volcanic rift zone along the East African Rift System, where previous studies have suggested a thick, strong, cold lithosphere (Craig et al., 2011; Foster and Jackson, 1998; Yang and Chen, 2010; Hodgson et al., 2017; Lavayssière et al., 2019) and ongoing unilateral propagation of the rift tips (Kolawole et al., 2021). A previous study (Hodgson et al., 2017) utilized the receiver function technique to map the spatial distribution of crustal-averaged Vp/Vs ratios but lacked constraints on the shallowest structure. Our results provide insight into the fundamental mechanism of strain distribution and localization along actively propagating rift segments. Ultimately, the approach may advance our understanding of how incipient divergent plate boundaries mature within active continental environments.

## 2 The Rukwa-Tanganyika Rift Zone

### 2.1 Pre-Rift Crystalline Basement

The crystalline crust of the Rukwa-Tanganyika Rift Zone (Fig. 1a) is mainly composed of metamorphic and igneous rocks of the Paleoproterozoic (1.85–1.95 Ga) Ubendian mobile belt (Fig. 1b), flanked by Archean crystalline rocks of the Bangweulu and Tanzania cratons and their overlying Neoproterozoic sedimentary sequences to the southwest and northeast respectively (Fig. 1b). The Ubendian Belt consists of several amalgamated NW-trending terranes defining the orogenic belt that accommodated the Paleoproterozoic collision events (2.025–2.1 Ga) between the Tanzania Craton and the Bangweulu Block. The terranes, comprising Ufipa, Katuma, Wakole, Lupa, Mbozi, Ubende, and Upangwa (Fig. 1b; Daly, 1988; Lenoir et al., 1994), are now exhumed due to long-term erosion and are bounded by steeply-dipping, ductile, amphibolite facies, strike-slip shear zones (Fig. 1b; Daly, 1988; Lenoir et al., 1994; Theunissen et al., 1996; Kolawole et al., 2018, 2021b; Lemna et al., 2019; Heilman et al., 2019; Ganbat et al., 2021). Their associated ductile fabrics are suggested to have influenced the development of post-Precambrian rift basins in the region (Wheeler and Karson, 1994; Theunissen et al., 1996; Klerkx et al., 1998; Boven et al., 1999; Heilman et al., 2019; Lemna et al., 2019; Kolawole et al., 2018, 2021a,b).

### 2.2 Phanerozoic Rifting History

The Rukwa-Tanganyika Rift Zone is defined by a system of NNW-to-NW-trending overlapping rift segments, consisting of the Tanganyika Rift, the Rukwa Rift to its southeast, and the ENE-trending Mweru-Wantipa Rift located just southwest of its southernmost sub-basin (Fig. 1). The rift zone records multiple phases of Phanerozoic tectonic extension, with the first phase occurring in the Late Permian to Triassic, the second phase beginning in the Late Jurassic but peaking in the Cretaceous, and the third phase initiating in the Late Oligocene and presently persisting (e.g., Delvaux, 1989, Roberts et al., 2012). Although studies show that all the rift segments are currently active (e.g., Daly et al., 2020; Hodgson et al., Lavayssiere et al., 2019; Heilman et al., 2019; Kolawole et al., 2021a), all the sub-basins do not record the three phases of Phanerozoic rifting (Delvaux,

1989; Morley et al., 1992, 1999; Muirhead et al., 2019; Shaban et al., 2023). In the Rukwa Rift, where there exist the only basement-penetrating boreholes to constrain seismic reflection interpretation, detailed mapping of the lateral extents of the Mesozoic and Cenozoic syn-rift sequences (Morley et al., 1992) and rift faulting patterns (Morley et al., 1992, 1999; Heilman et al., 2019; Kolawole et al., 2021b) show that the Rukwa Rift progressively elongated northwestwards and southeastwards over the rift phases.

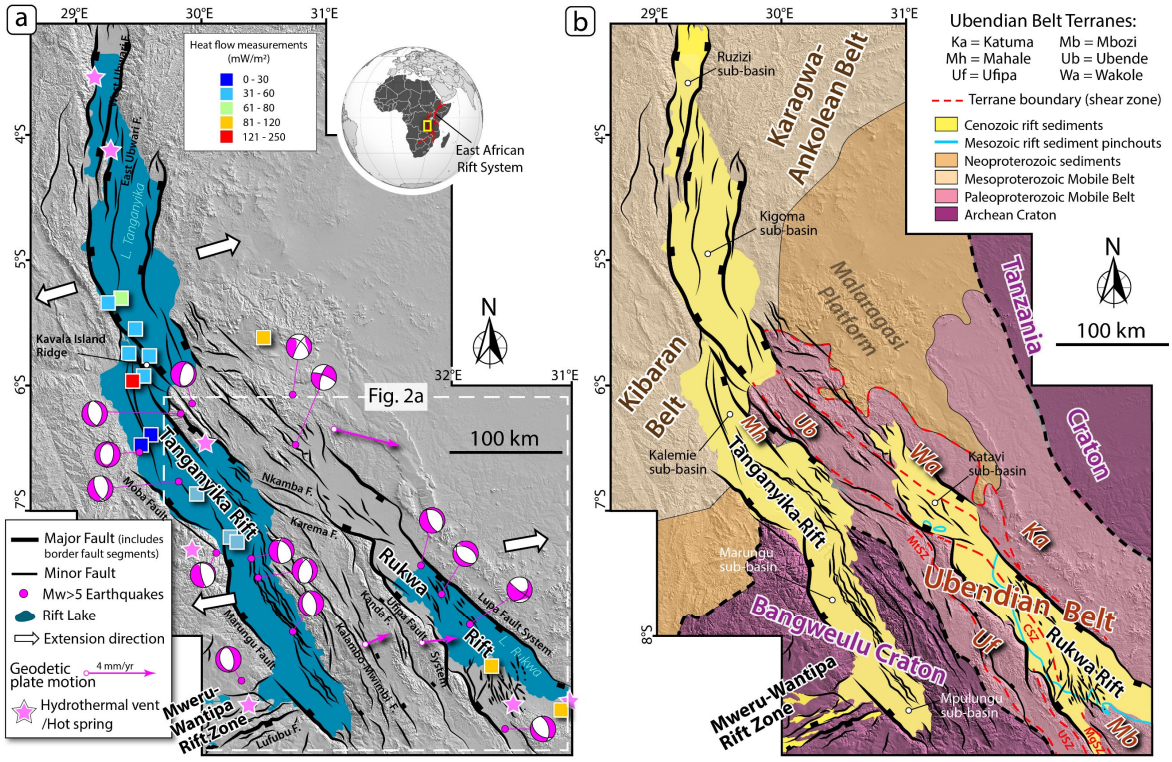


**Figure 1**. (**a**) Tectonic map of the Rukwa-Tanganyika Rift Zone showing the rift faults (Morley et al., 1999; Muirhead et al., 2019; Kolawole et al., 2021a). Focal mechanisms and epicenters of Mw >5 earthquakes from National Earthquake Information Center (NEIC) catalog (1976–2018) obtained through the United States Geological Survey website (https://earthquake.usgs.gov/earthquakes/search/). Geodetic plate motion vectors are from Stamps et al. (2008). Regional extension directions are from Delvaux and Barth (2010) for the northern Tanganyika Rift and Lavayssière et al. (2019) for the southern Tanganyika and Rukwa rift basins. Heat flow measurements and their locations are from Jones (2020). Sites of hot springs/hydrothermal vents are from Tiercelin et al. (1993), Lavayssière et al. (2019), Jones (2020), and Mulaya et al. (2022). (**b**) Geological map of the region, showing the cratons, mobile belts, terranes of the Ubendian Belt and shear zones, and Cenozoic syn-rift sediments (modified after Hanson, 2003; Delvaux et al., 2012; Kolawole et al., 2021a,b; Ganbat et al., 2021). Exhumed Precambrian shear zones (Heilman et al., 2019): CSZ, Chisi Shear Zone; MgSZ, Mughese Shear Zone; MtSZ: Mtose Shear Zone; USZ: Ufipa Shear Zone.

The Cretaceous rifting event included reactivated faulting, tectonic subsidence, and sedimentation in the Rukwa Rift and Luama Rift (e.g., Veatch, 1935; Delvaux, 1991; Roberts et al., 2012). Cenozoic rifting initiated the development of rift basins as segments of the 'East African Rift System,' featuring the reactivation of the Rukwa Rift and the development of the

Tanganyika and the Mweru-Wantipa rift segments (e.g., Morley et al., 1999; Delvaux et al., 2001; Chorowicz, 2005; Daly et al., 2020). Crustal thickness across the rift zones range 31.6 – 42 km (Hodgson et al., 2017; Njinju et al., 2019) and lithosphere thickness 130 – 170 km (Njinju et al., 2019). The modern regional extension direction is N74°E in the northern Tanganyika Rift (Delvaux and Barth, 2010) and N80°E in the southern Tanganyika and Rukwa rifts (Lavayssière et al., 2019) (Fig. 1a).

### 2.3 Rift Faulting and Seismicity Patterns

The Tanganyika Rift basin is bounded by a system of large border faults that alternate polarity along-trend of the basin (Versfelt and Rosendahl, 1989) and include the Marungu Fault, the Kavala Island Ridge Faults, the West and East Ubwari Faults, and the Moba Fault (Fig. 1a), whereas the large graben of the Rukwa Rift basin is bounded by laterally continuous border fault systems of the Lupa Fault to the northeast and Ufipa Fault to the southwest (Heilman et al., 2019). The Ufipa Horst represents the intervening basement block between the southern Tanganyika Rift and the Rukwa Rift and is accommodating active deformation as evidenced by the ca. 100-km long scarps of the Kanda and Kalambo-Mwimbi Faults (Fig. 1a; Delvaux et al., 2012; Kolawole et al., 2021). Moreover, two prominent fault scarps extend westward from the Rukwa Rift tip across a basement region to the eastern margins of the central Tanganyika Rift (Nkamba and Karema Faults; Fig. 1a). The deformation zone of the Mweru-Wantipa Rift hosts a ca. 50-km-wide parallel fault cluster that defines its southeastern margin within which the Lufuba Fault appears to have the greatest escarpment height (Fig. 1a).

The entire Rukwa-Tanganyika Rift Zone records widespread seismicity (Figs. 2a, c–d) that extends beyond 42 km depth, indicating that the seismogenic layer of the rift includes the uppermost mantle (Fig. 2c–e; Lavayssière et al., 2019). The events define clusters with focal mechanism solutions that suggest steep, deep-rooting, large normal faults (Lavayssière et al., 2019), and highlight localized active crustal deformation zones beneath Tanganyika Rift, Rukwa Rift, the Ufipa Horst, and the Mweru-Wantipa Rift (Fig. 1a). Across the rift zone, the earthquakes commonly initiate at the middle-crust and extend down into the lower crust, except the northwestern tip of the Rukwa Rift (Katavi sub-basin; Figs. 2a, 2d) where the earthquakes primarily localized within the upper crust (Lavayssière et al., 2019). More interestingly, the axis of the Rukwa Rift has sparse seismicity. Seismicity clusters at the Rukwa Rift tip extend beyond the margins of the basin sediments, continuing outboard into the regions of the exposed pre-rift basement (Figs. 2a and 2d). In the Tanganyika Rift, earthquakes mostly cluster within the rift axis and extend along most of the rift length (Figs. 2a and 2c). Heat flow measurements in the rift zone show thermal anomalies in the central Tanganyika Rift (<30 to 250 mW/m2), the south-central region of the Rukwa Rift (81 – 120 mW/m2), and within the basement region ahead of the northwestern tip of the Rukwa Rift (81 – 120 mW/m2) (Fig. 1a; Jones, 2020). The thermal anomaly north of the Rukwa Rift tip occurs near NW-trending fault splays and Mw>5 earthquake epicenters within the basement region. Furthermore, hydrothermal vent and hot spring locations coincide with the border fault zones of the Tanganyika Rift and the south-central part of the Rukwa Rift (Fig. 1a; Tiercelin et al., 1993; Lavayssière et al., 2019; Jones, 2020).

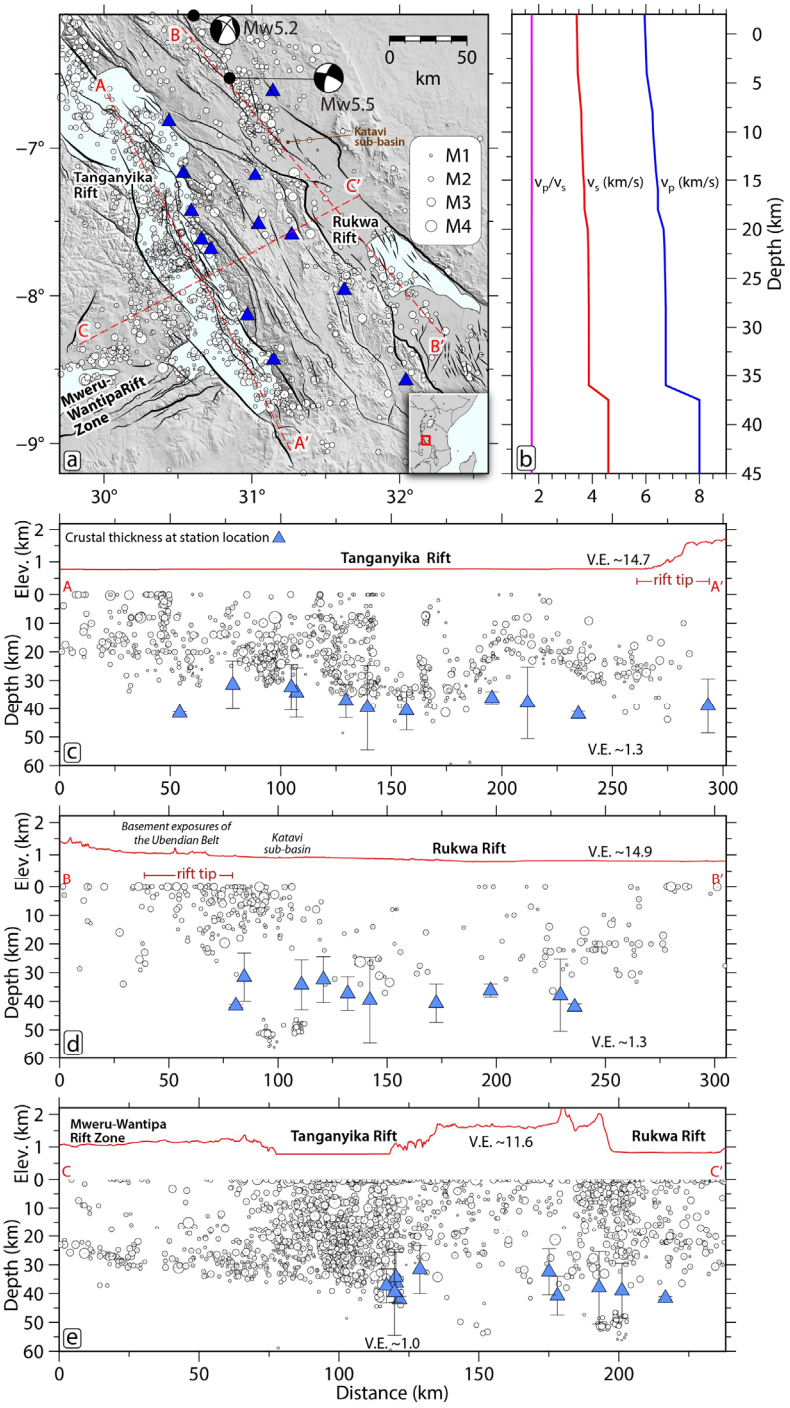


**Figure 2**. (**a**) Map of the southern Tanganyika and Rukwa rift zone showing the local seismicity (white circles; from TANGA14 array – network ZV, Lavayssière et al., 2019) scaled by magnitude. The black dots represent events used in the inversion. Previously deployed

broadband seismometers are the blue triangles. Black lines are faults; the thicker black lines highlight border faults. Red dashed lines are locations of seismicity profiles in c-e. Inset map shows the relative location in East Africa. (**b**) Starting model used in the seismic tomographic inversion (from Lavayssière et al., 2019). (**c** - **e**) Elevation and depth profiles showing projected seismicity from Lavayssière et al. (2019) and estimated Moho depths from Hodgson et al. (2017) along and across the rifts. Profiles A-A' and B-B' only show earthquakes within 25 km.

### 2.4 Active Deformation Across the Rift Overlap Zones

At a regional scale, the Rukwa and Tanganyika rift basins are separated by an elevated region of pre-rift basement with widespread exposures of Precambrian metamorphic rocks (Figs. 1a-b; Kolawole et al., 2021a). This region of rift overlap, described as an overlapping parallel-to-oblique 'rift interaction zone' (Kolawole et al., 2021), is characterized by historical seismicity and active faults that deform the modern surface (Delvaux et al., 2001; Lavayssière et al., 2019; Kolawole et al., 2021a). The faults include the WNW-trending Karema and Nkamba faults, which splay westwards from the Rukwa Rift tip (Fig. 1a; Fernandez-Alonso et al., 2001; Kolawole et al., 2021a), and NW-trending faults that extend northwards towards the margin of the northern Tanganyika Rift (Kolawole et al., 2021a). The longitudinal surface relief morphology of the southern Tanganyika Rift shows a significantly steeper gradient than that of the Rukwa Rift tip ('rift tip' in Fig. 2c versus 2d). Overall, the current stage of evolution of the rift interaction zone based on the relief profile, stream flow patterns, and drainage morphologies is inferred to be partially breached (Kolawole et al., 2021a). The Mweru-Wantipa Rift extends eastward and appears to be hard-linked with the border fault of the western flank of the southern tip of the Tanganyika Rift. The region between the two rifts defines an overlapping orthogonal rift interaction zone, and the continuation of Lake Tanganyika into the Mweru-Wantipa Basin and the apparent coalescence of the rift floors of the two basins suggest a breached rift interaction zone between them (Kolawole et al., 2021a).

## 3 Body-Wave Tomography

### 3.1 Seismic Data

We focus on waveform data recorded by the TANGA14 array, comprising 13 broadband seismographs deployed along the Ufipa Plateau for 15 months from June 2014 through September 2015 (Hodgson et al., 2017). Using the origin times from the local earthquake catalog developed by Lavayssière et al. (2019) comprising 2213 events (Fig. 2a), we download the associated waveforms using the facilities of the EarthScope Consortium. The waveforms were then filtered with a Butterworth filter to accentuate the earthquake signal in the frequency band used in Lavayssière et al. (2019): 2 – 15 Hz. First arrival times for both P and S waves were manually picked on filtered seismograms resulting in 3187 P times from 1277 earthquakes (resp. 3121 S times from 1261 earthquakes). We only made the travel time picks when the phases were clear and impulsive. We do not record uncertainty in arrival times during picking, nor do we pick multiple times to estimate the data variance.

### 3.2 Backprojection Tomography

Using our manually picked P and S arrival times, we develop 3D P and S velocity models for the Tanganyika-Rukwa region via nonlinear back-projection travel time inversion (Hole, 1992; Hole et al., 2000). Our preferred initial velocity model for the area is the 1D P and S velocity model developed by Lavayssière et al. (2019). We parameterize the model space using a fixed 5 km grid spacing with dimensions of 425 km x 435 km x 50 km. The bottom right corner of the model is 29.1651º E and -9.6764º S and extends from 7 km above sea level to 43 km depth. Therefore, we use the actual station elevations without needing static corrections. The travel time predictions in the model are calculated using a finite-difference solution for the Eikonal equation (Vidale, 1990), which allows travel times to be computed for all grid points in the model. Ray paths are then simultaneously traced for any number of source-receiver pairs using the gradient of the travel time field. Due to the reciprocity in the travel time computation, we treat the receivers as sources, thus, requiring only 13 forward computations in each iteration. Following the forward calculation, we iteratively update the models, $k$, at each grid point, $j$, as follows:

$$u_{k+1}^{j} = u_{k}^{j} + \delta u_{k}^{j}, \tag{1}$$

where the slowness perturbations, $\delta u$, are calculated using simple back-projection as the average of the neighborhood ray paths, i.e.,

$$\delta u_{k}^{j} = \frac{1}{N} \sum_{cells} \sum_{rays} \frac{\delta t_{ray}}{l_{ray}}, \tag{2}$$

with $\delta t$ and $l$ being the associated traveltime residual and raypath length for the associated ray. We further smooth the perturbations once they are determined for all grid points in the model using a 3D moving average filter to control the spatial resolution and stabilize the inversion. This procedure is like higher-order Tikhonov regularization in the least squares nonlinear inversion. We gradually reduce the size of the smoothing dimension after every five iterations to increase the spatial resolution of the model. The final smoothing size of our model from the 26th iteration is 5 x 5 x 3 grid points. Subsequent iterations do not have substantially lower misfits but become contaminated by noise (Fig. S1). Finally, the Vp/Vs ratio is obtained by dividing the P and S velocity models.

### 3.3 Model Reliability Assessment

To assess the model uncertainty, we employ a combination of ray coverage maps, classical checkerboard reconstruction tests, a custom synthetic model reconstruction test, and real data inversion using different starting models to determine areas of the model reliable enough for interpretation (Figs. 3 – 5 and S2 – S18). We generate the checkerboard models by adding 3D sinusoid functions to the initial velocity model (Fig. 2b) using similar magnitudes in the amplitudes of the real, inverted model (Fig. 5). The observed travel time dataset is computed in the checkerboard model and then inverted using the unperturbed starting model. We do not add noise to the synthetic datasets. We also test different sizes of the anomalies (Figs. S4 – S15).

Based on the results from the artificial reconstructions, we define a polygon (e.g., Figs. 4 and 5) in the model space where the model parameters are reasonably resolved and note that the checkerboard anomalies are accurately recovered in areas of the polygon with zero or sparse ray coverage. Also, we developed and inverted a custom synthetic model (Figs. 3 and 4) based on the vital features we interpret in our final preferred model (Fig. 5) at the edge of the polygon where ray coverage is sparse or lacking (Fig. S2).

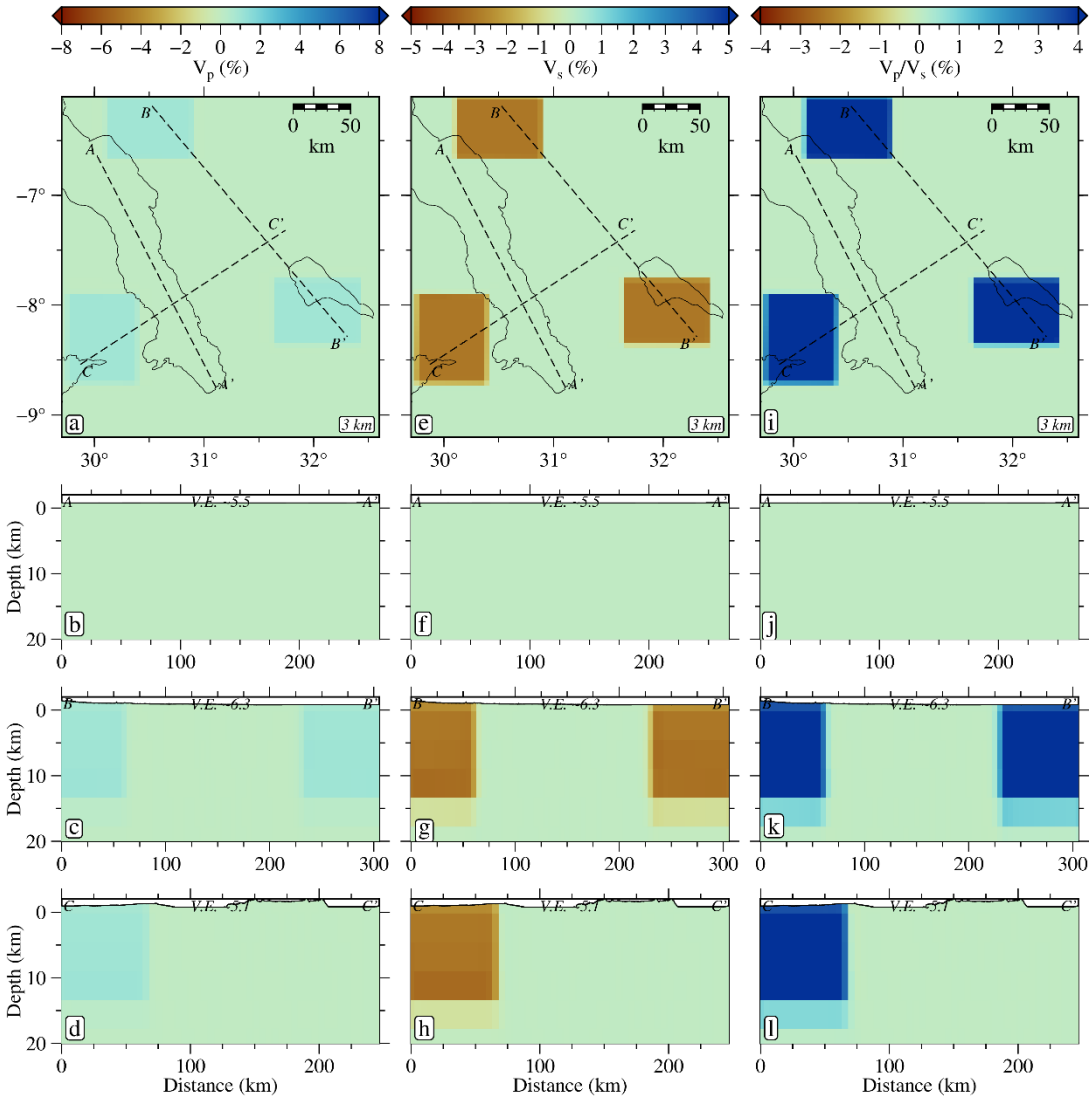


**Figure 3**. True custom synthetic model generated by perturbing the P (1% increase) and S (3% decrease) velocity models to generate three Vp/Vs (~4 % increase) anomalies. (**a**) 3 km depth slice through the P wave velocity model. Dashed black lines show the profile locations in b-d. (**b** – **d**) Profiles of the P wave velocity model. (**e** – **h**) Same as a-d but for the S wave velocity model. (**i** – **l**) Same as a-d but for the Vp/Vs ratios.

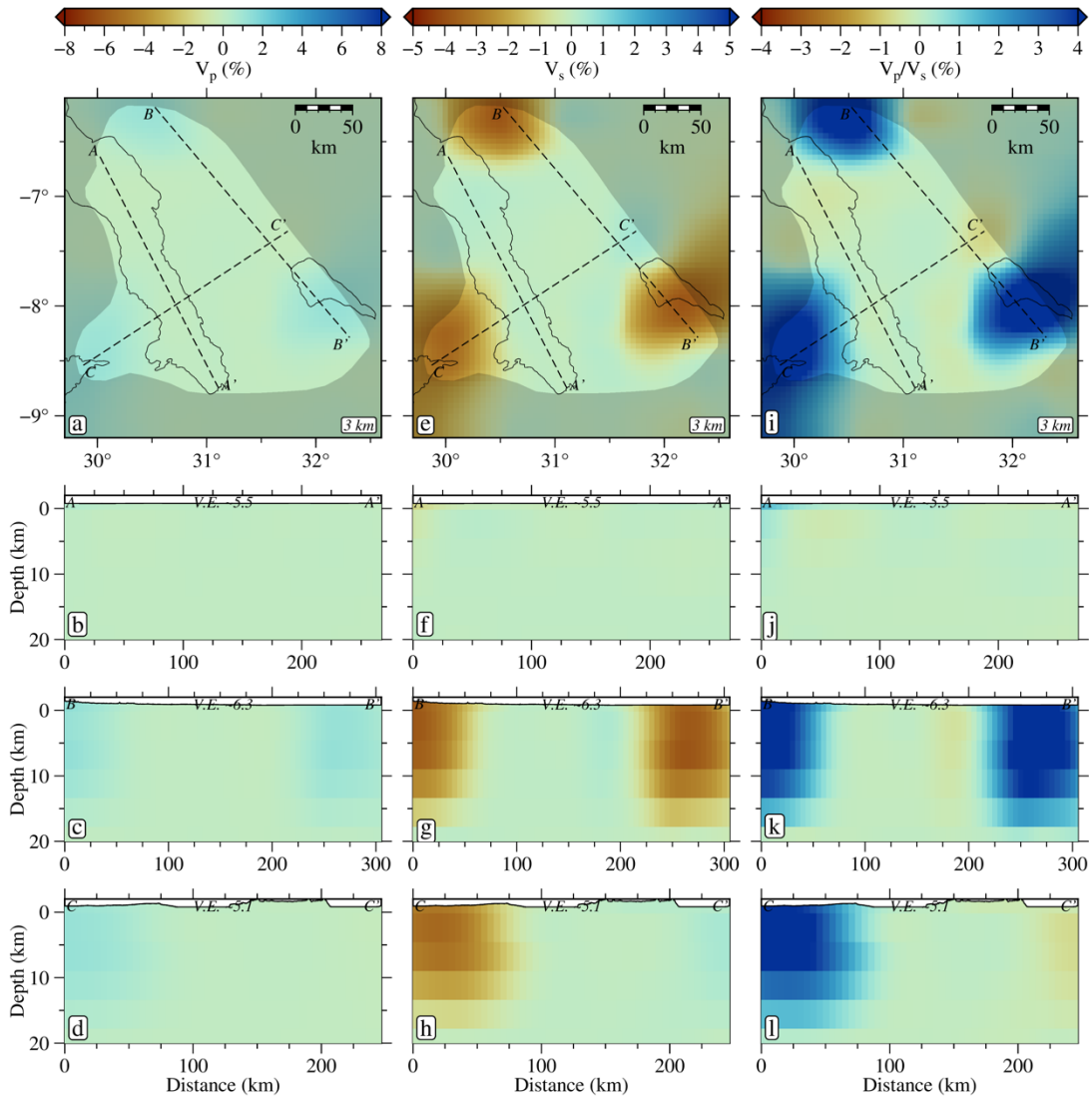


**Figure 4**. Recovered custom synthetic model from Fig. 3. (**a**) 3 km depth slice through the P wave velocity model. Dashed black lines show the profile locations in b-d. Unreliable areas of the model are lightly grayed out. (**b** – **d**) Profiles of the P wave velocity model. (**e** – **h**) Same as a-d but for the S wave velocity model. (**i** – **l**) Same as a-d but for the Vp/Vs ratios.

The synthetic model comprises three high Vp/Vs (~4 % increase) anomalies generated by perturbing the P (1 % increase) and S (3 % decrease) velocity model and extending from 2 km above zero to 13 km depth in the model space, with the following horizontal dimensions: 80 by 60 km at the north, 80 by 60 km at the southeast, and 65 by 85 km at the southwest. The inversion results show good recovery of the anomalies with some smearing outside our predefined polygon (Fig. 4). To further assess

the reliability of these features in the real model (Fig. 5), we perform two other inversions of the real data using two different 3D initial velocity models from Celli et al. (2020) and van Herwaarden et al. (2023). A comparison of the results of all three starting models (Figs. S16 – S18) shows that the Vp/Vs anomalies are robust.

### 3.4 Preferred Inversion Result

We present our preferred velocity models as perturbations (Fig. 5) relative to the starting models used in the inversion (Fig. 2b). The 5 km model grid spacing makes our selection of the 3 km depth maps (Figs. 5a, 3e, and 3i) representative of the average uppermost crustal structure of the model in the region, as can be verified in the cross-sectional profiles of Fig. 3. The overall distribution of upper crustal velocities generally reflects the near-surface geology, which serves as a primary constraint for assessing the quality of the models. Our results show that slower Vp and Vs are collocated with the sedimentary basins of the southern Tanganyika and Rukwa rifts. Relatively lower velocities continue along a narrow ESE-trending zone from the Tanganyika Rift to the northern end of the Rukwa Rift, following the Nkamba and Karema faults. The Ufipa Horst separating the Tanganyika and Rukwa rifts also shows localized zones of Lower Vp, collocated with areas of pervasive surface faulting (Fig. 5a). However, unlike the Vp distribution, the Ufipa Horst is better defined in the Vs model, demonstrated by the relatively higher values and structural continuity (Figs. 5e and h). Within the eastern section of the Mweru-Wantipa Rift and further east towards the southern Tanganyika Rift, we observe moderate Vp anomalies collocated with moderate-to-low Vs anomalies (Figs. 5a – b, e – f). Overall, the rift flanks and zones of widespread exposure of the pre-rift basement exhibit relatively higher Vp and Vs.

The Vp/Vs ratio map (Fig. 5i) and cross-sections (Figs. 5j – l) show zones of anomalously high values that are restricted to upper-crustal depths, the most prominent of which are A1: an anomaly at the northwestern end of the Rukwa Rift, an area dominated by basement exposures and distributed faulting, A2: a broad anomaly extending across the eastern end of the Mweru-Wantipa Rift through the transfer zone into the Tanganyika Rift, and A3: an anomaly in the southeastern interior of the Rukwa Rift, collocated with the Ufipa Fault and the intra-basement Chisi Shear Zone (Fig. 1b). These highest Vp/Vs anomalies commonly continue downward to 10 km or deeper (Figs. 5k – l) but our investigation focuses on the upper crust.

## 4 Discussion

Fault-related damage and distributed brittle deformation in the crystalline crust often create decreased bulk crustal density regions, manifested as anomalously low Vs and Vp/Vs zones (Allam et al., 2014; Fang et al., 2019). Also, regions where brittle damage allows the upwelling of hydrothermal fluids in the upper crust are associated with relatively higher Vp/Vs values (Hua et al., 2019). In active rift settings with absent surface volcanism, understanding the spatial distribution of upper-crustal seismic velocities permits the identification of mechanically weakened zones where tectonic strain may be preferentially localized. Delineating these near-surface structures will help better predict ground motion amplification during large earthquakes (Ajala and Persaud, 2021; Cormier and Spudich, 1984).

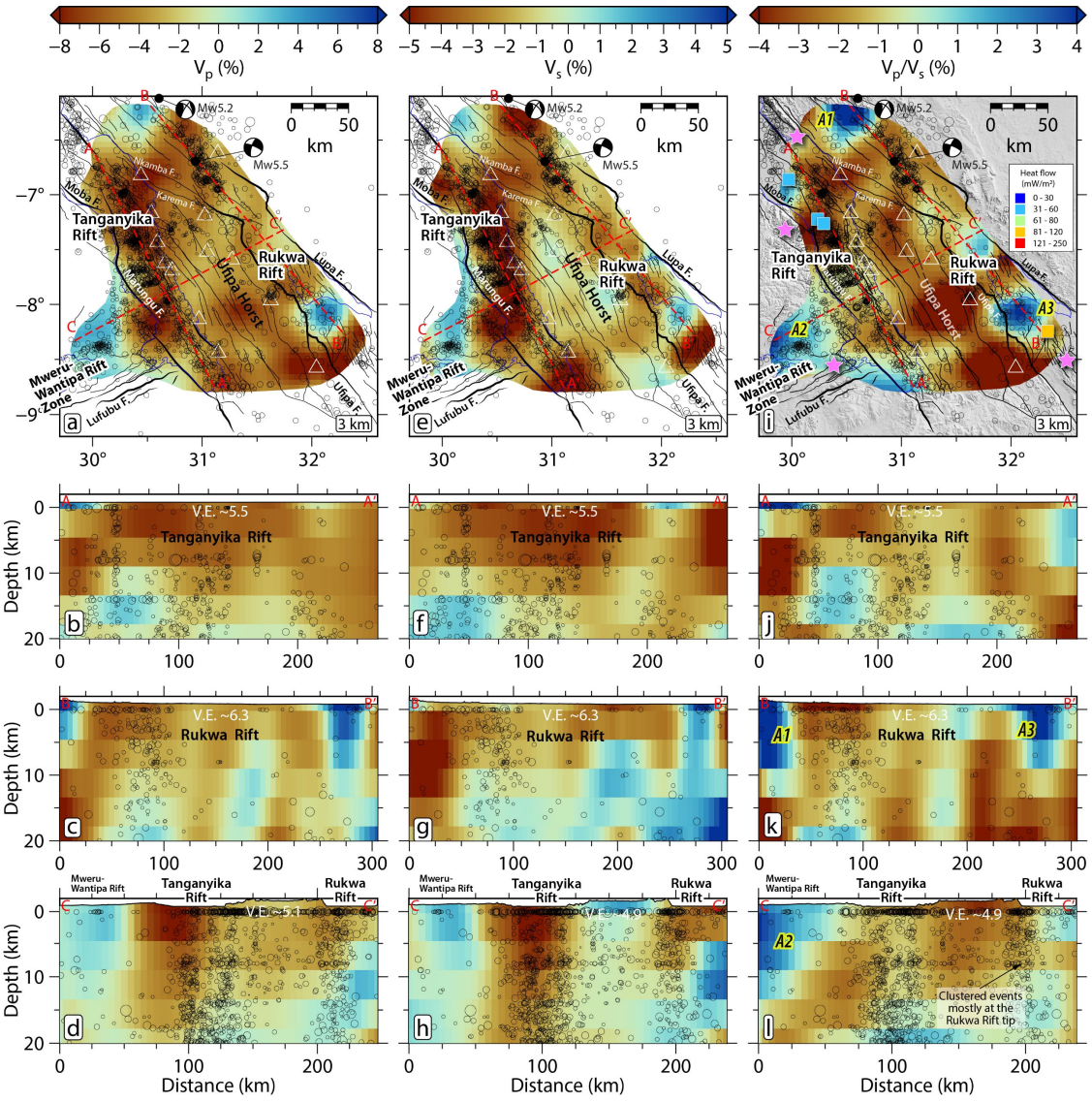


**Figure 5**. Maps and profiles through the tomographic models showing the perturbations relative to the starting models in Fig. 2b. (**a**) 3 km depth slice through the P wave velocity model. Unreliable areas of the model are not shown. Dashed black lines show the profile locations in b-d. (**b** – **d**) Profiles of the P wave velocity model. (**e** – **h**) Same as a-d but for the S wave velocity model. (**i** – **l**) Same as a-d but for the Vp/Vs ratios. Absolute values of the model parameters are shown in Fig. S16. Note that the geothermal center near anomaly A1 is north of latitude 6°S which is outside of the map coverage (see Fig. 1a).

Two of the three areas of the highest upper-crustal Vp/Vs ratios (A1 and A2) occur at rift tips where syn-rift sedimentary cover is thinnest, and basement exposures dominate the surface geology (Figs. 1b and 3i). These anomalies occur at or near

geothermal anomalies (Fig. 1a) and are collocated with earthquake clusters and distributed normal faults. The anomalous seismicity cluster at the tip indicates the focus of active brittle deformation of the crystalline crust in a region lacking well-developed rift basins. At the Rukwa Rift tip and further to the northwest, the faulting pattern is generally characterized by distributed faults that extend outboard from the Rukwa Rift border faults (Fig. 1a). At the Mweru-Wantipa Rift tip, the rift faults mainly cluster near the southern margin. Thus, we interpret the occurrence of the high upper-crustal Vp/Vs anomalies at the modern rift tips to represent a localization of mechanically weakened crystalline crust.

Localization of mechanically weakened crust at active rift tips reflects a critical process facilitating the growth of continental rift systems analogous to microfracture propagation driven by high-stress concentrations at the crack tips (e.g., Kranz, 1979; Olson, 2004). Similarly, relatively large stress concentrations between interacting microcrack tips (Kranz, 1979) agrees with interpretation of stress concentrations within rift interaction zones that separate propagating rift tips (Kolawole et al., 2023). Here, the northwestern tip of the Rukwa Rift is characterized by geomorphic features and tectonic deformation patterns that suggest an ongoing northwestward propagation towards the central and northern Tanganyika Rift (Kolawole et al., 2021a). The earthquake clusters at the Rukwa and Mweru-Wantipa rift tips (Fig. 2a) indicate that tectonic stresses and elastic strain concentrations are focusing at the rift tip zones. These earthquakes are likely induced by bending stresses and the associated plastic strain along the rift tip's flexural margin (Fig. 6a). Several studies have demonstrated that crustal bending due to accumulated fault displacement, glacial unloading, thermal subsidence, or sediment load induced crustal subsidence can focus significant strain in the upper crust, leading to brittle failure of the crust (e.g., Goetze and Evans, 1979; Stein et al., 1979; Nunn, 1985). Here, long-term accrual of fault displacement and sediment loading on the hanging walls of the Lupa and Ufipa border faults causes crustal down-flexure in the rift axis and contemporaneous crustal upwarping at the rift tips (Fig. 6a). The upwarping of the basement at the rift tips induces significant extensional strain in the upper part of the brittle lithosphere, which explains the localized clusters of earthquakes at the rift tip, best expressed at the northwestern tip zones of the Rukwa Rift (Figs. 2a, 2d). Thus, damage clustering at the rift tip is a relevant fundamental process that may facilitate mechanical weakening at the tips of active continental rifts.

However, we note that the seismicity clusters are not collocated with the high Vp/Vs ratio anomalies but occur near their margins (Figs. 5i). We interpret this to indicate a transition from one frictional stability domain to another within the upper crust. Fluid saturation and pressure may decrease the effective normal stresses on basement faults and fractures, leading to their failure. Nevertheless, the brittle failure may be aseismic or seismic depending on the lithology of the fault rocks (and host rocks) and loading conditions (e.g., Blanpied et al., 1991; Carpenter et al., 2011; Kolawole et al., 2019). Given the same loading conditions around the rift tip, we infer that pervasive compositional alteration (likely hydrothermal) within the areas of highest Vp/Vs could have created compositional variations that promote aseismic failure within the zones of highest Vp/Vs ratios (D1 in Fig. 6a) as opposed to their surrounding regions that are failing by seismogenic deformation (zone D2). The Vp/Vs anomaly

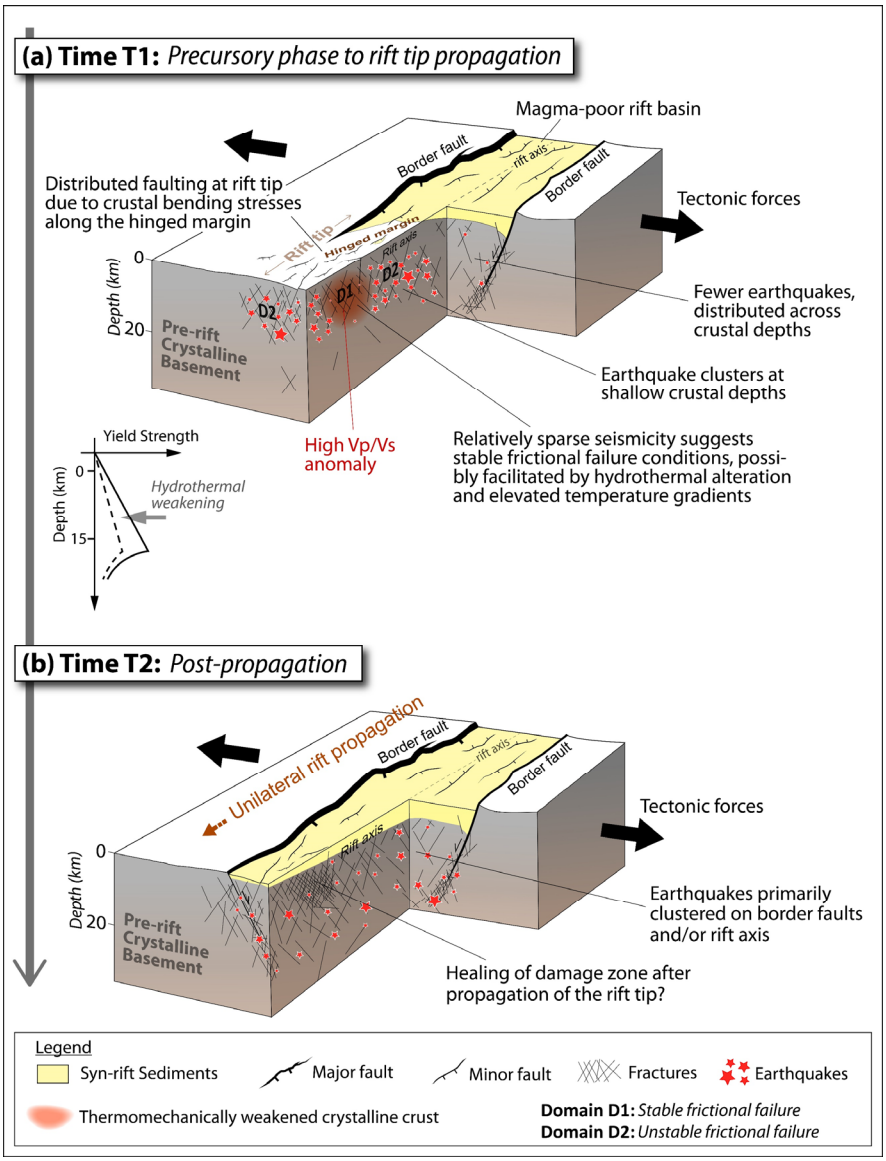


**Figure 6**. **(a – b)** Cartoons showing the newly proposed model of crustal strain accommodation during the unilateral propagation phase of an active continental rift tip as suggested by the results of this study.

A3 within the Rukwa Rift is collocated with an area of relatively less intra-rift fault occurence (Fig. 5i). However, this anomaly is in the hanging wall of the Ufipa border fault near a known geothermal anomaly (Jones, 2020). Since A3 is confined to <5 km depth (Fig. 5k), it also likely represents a compositionally-altered and mechanically weakened section of the border fault

and its hanging wall block, similar to velocity anomalies observed near geothermal field of active rifts elsewhere (e.g., Hauksson and Unruh, 2007).

Published models for rift linkage demonstrate that rift basins can propagate laterally and interact when in proximity (e.g., Allken et al., 2012; Corti, 2012; Molnar et al., 2019; Nelson et al., 1992; Zwaan et al., 2016; Zwaan and Schreurs, 2020; Neuharth et al., 2021; Kolawole et al., 2021a). Studies of natural rifts also show that inherited crustal mechanical barriers, non-optimal rift interaction zone geometry, or unfavorable tectonic stress distribution can stall lateral rift propagation (e.g., van Wijk and Blackman, 2005; Kolawole et al., 2022, 2023; Shaban et al., 2023). Numerical models show that the stalling of a laterally propagating rift tip creates a local stress concentration zone (van Wijk and Blackman, 2005; Le Pourhiet et al., 2018). Our study presents evidence from a natural rift for the first time, revealing localized crustal weakening at a laterally propagating continental rift tip. We propose a model for lateral rift propagation whereby the inception of propagation is marked by the development of localized brittle damage (Time T1, Fig. 6a). Subsequently, the weakened crust gives way to a lengthened rift basin (Time T2, Fig. 6b).

## Conclusions

To understand how tectonic strain is accommodated along actively propagating magma-poor continental rifts, we constructed three-dimensional velocity models of the crystalline crust beneath the Rukwa-Tanganyika Rift Zone. The results show anomalously high Vp/Vs ratio anomalies at the current rift tips and rift interaction zones, representing, for the first time, geophysical evidence demonstrating that an initial crustal softening of the rift tip may be required to initiate unilateral rift propagation. We determine that brittle damage due to bending stresses and associated strain, potentially compounded by hydrothermal weakening at the rift tip's flexural margin facilitates the observed pronounced softening. These new results provide compelling insight into how continental rift tips propagate, link, and coalesce to form continuous axial rift floors — a necessary ingredient for initiating large-scale continental break-up axis.

## Acknowledgments

This project was supported by funds from the Columbia Climate School awarded to Folarin Kolawole. We thank Finnigan Illsley-Kemp for comments that helped to improve the earlier version of the manuscript. Some figures are plotted using GMT (Wessel et al., 2019).

## Author contributions

F.K. and R.A. conceptualized the project. R.A. performed the modeling. F.K. and R.A. interpreted the results. F.K. wrote the manuscript. R.A. revised the manuscript.

## Competing interests

The authors declare no competing interests.

## Open Research

Computer programs and files to reproduce our results are in Ajala and Kolawole (2023).

**References**


Aanyu, K. and Koehn, D., 2011. Influence of pre-existing fabrics on fault kinematics and rift geometry of interacting segments: analogue models based on the Albertine Rift (Uganda), Western Branch-East African Rift System. Journal of African Earth Sciences, 59(2-3), pp.168-184.

Acocella, Faccenna, Funiciello and Rossetti, 1999. Sand-box modelling of basement-controlled transfer zones in extensional domains. Terra Nova, 11(4), pp.149-156.

Ajala, R., and Kolawole, F. (2023). Reproducibility material for crustal softening at propagating rift tips. Retrieved from https://doi.org/10.5281/zenodo.8302196

Ajala, R. and Persaud, P. (2021). Effect of Merging Multiscale Models on Seismic Wavefield Predictions Near the Southern San Andreas Fault. Journal of Geophysical Research: Solid Earth, 126, 1-23.

Allam, A. A., Ben-Zion, Y., Kurzon, I., and Vernon, F., 2014. Seismic velocity structure in the Hot Springs and Trifurcation areas of the San Jacinto fault zone, California, from double-difference tomography. Geophysical Journal International, 198, 978-999.

Allken, V., Huismans, R.S. and Thieulot, C., 2012. Factors controlling the mode of rift interaction in brittle-ductile coupled systems: A 3D numerical study. Geochemistry, Geophysics, Geosystems, 13(5).

Blanpied, M.L., Lockner, D.A. and Byerlee, J.D., 1991. Fault stability inferred from granite sliding experiments at hydrothermal conditions. Geophysical Research Letters, 18(4), pp.609-612.

Brune, S., Kolawole, F., Olive, J.A., Stamps, D.S., Buck, W.R., Buiter, S.J., Furman, T. and Shillington, D.J., 2023. Geodynamics of continental rift initiation and evolution. Nature Reviews Earth & Environment, 4(4), pp.235-253.

Carpenter, B.M., Marone, C. and Saffer, D.M., 2011. Weakness of the San Andreas Fault revealed by samples from the active fault zone. Nature Geoscience, 4(4), pp.251-254.

Celli, N. L., Lebedev, S., Schaeffer, A. J., and Gaina, C. (2020). African cratonic lithosphere carved by mantle plumes. Nature Communications, 11(92), 1-10.

Chen, Y.L., Ni, J., Shao, W. and Azzam, R., 2012. Experimental study on the influence of temperature on the mechanical properties of granite under uni-axial compression and fatigue loading. International Journal of Rock Mechanics and Mining Sciences, 56, pp.62-66.

Cormier, V. F. and Spudich. (1984). Amplification of ground motion and waveform complexity in fault zones: examples from the San Andreas and Calaveras Faults. Geophys. J. R. astr. Soc., 79, 135–152.

Corti, G., 2004. Centrifuge modelling of the influence of crustal fabrics on the development of transfer zones: insights into the mechanics of continental rifting architecture. Tectonophysics, 384(1-4), pp.191-208.

Craig, T. J., Jackson, J. A., Priestley, K., and McKenzie, D. (2011). Earthquake distribution patterns in Africa: Their relationship to variations in lithospheric and geological structure, and their rheological implications. Geophysical Journal International, 185(1), 403–434. https://doi.org/10.1111/j.1365-246X.2011.04950.x

Delvaux, D., 1989. The Karoo to recent rifting in the western branch of the East-African Rift System: a bibliographical synthesis. In: Mus. Roy. Afr. Centr., Tervuren (Belg.), Dept. Geol. Min., Rapp. Ann, 1990, 1991, pp. 63–83.

Delvaux, D., and Barth, A. (2010). African stress pattern from formal inversion of focal mechanism data. Tectonophysics, 482(1–4), 105–128. https://doi.org/10.1016/j.tecto.2009.05.009.

Delvaux, D., Kervyn, F., Macheyeki, A. S., and Temu, E. B. (2012). Geodynamic Significance of the TRM Segment in the East African Rift (W-Tanzania): Active Tectonics and Paleostress in the Ufipa Plateau and Rukwa basin. J. Struct. Geology. 37, 161–180.

Fang, H., Yao, H., Zhang, H., Thurber, C., Ben-Zion, Y. and van der Hilst, R.D., 2019. V p/V s tomography in the southern California plate boundary region using body and surface wave traveltime data. Geophysical Journal International, 216(1), pp.609-620.

Foster, A. N., and Jackson, J. A. (1998). Source parameters of large African earthquakes: Implications for crustal rheology and regional kinematics. Geophysical Journal International, 134(2), 422–448. https://doi.org/10.1046/j.1365-246x.1998.00568.x

Gaherty, J.B., Zheng, W., Shillington, D.J., Pritchard, M.E., Henderson, S.T., Chindandali, P.R.N., Mdala, H., Shuler, A., Lindsey, N., Oliva, S.J. and Nooner, S., 2019. Faulting processes during early-stage rifting: Seismic and geodetic

analysis of the 2009–2010 Northern Malawi earthquake sequence. Geophysical Journal International, 217(3), pp.1767-1782.

Ganbat, A., Tsujimori, T., Boniface, N., Pastor-Galán, D., Aoki, S. and Aoki, K., 2021. Crustal evolution of the Paleoproterozoic Ubendian Belt (SW Tanzania) western margin: a Central African Shield amalgamation tale. Gondwana Research, 91, pp.286-306.

Goetze, C. and Evans, B., 1979. Stress and temperature in the bending lithosphere as constrained by experimental rock mechanics. Geophysical Journal International, 59(3), pp.463-478.

Hanson, R.E., 2003. Proterozoic geochronology and tectonic evolution of southern Africa. Geological Society, London, Special Publications, 206(1), pp.427-463.

Hauksson, E. and Unruh, J. (2007). Regional tectonics of the Coso geothermal area along the intracontinental plate boundary in central eastern California: three-dimensional Vp and Vp/Vs models, spatio-temporal seismicity patterns, and seismogenic deformation, Journal of Geophysical Research, 112(B6), 1-24.

Heilman, E., Kolawole, F., Atekwana, E. A., and Mayle, M. (2019). Controls of Basement Fabric on the Linkage of Rift Segments. Tectonics 38 (4), 1337–1366. doi:10.1029/2018tc005362.

Hodgson, I., Illsley-Kemp, F., Gallacher, R., Keir, D., Ebinger, C. J., and Mtelela, K. (2017). Crustal Structure at a Young Continental Rift: A Receiver Function Study from the Tanganyika Rift. Tectonics, 36, 1-17.

Hole, J. A. (1992). Nonlinear high-resolution three-dimensional seismic travel time tomography. Journal of Geophysical Research: Solid Earth, 97(B5), 6553-6562. http://dx.doi.org/10.1029/92JB00235

Jones, D. J. R. (2020). A summary of the East Africa Rift Temperature and Heat flow Model (EARTH). British Geological Survey Open Report, OR/20/006. 24pp.

Kolawole, F., Firkins, M.C., Al Wahaibi, T.S., Atekwana, E.A. and Soreghan, M.J., 2021a. Rift interaction zones and the stages of rift linkage in active segmented continental rift systems. Basin Research, 33(6), pp.2984-3020.

Kolawole, F., Johnston, C.S., Morgan, C.B., Chang, J.C., Marfurt, K.J., Lockner, D.A., Reches, Z. and Carpenter, B.M., 2019. The susceptibility of Oklahoma's basement to seismic reactivation. Nature Geoscience, 12(10), pp.839-844.

Kolawole, F., Phillips, T.B., Atekwana, E.A. and Jackson, C.A.L., 2021b. Structural inheritance controls strain distribution during early continental rifting, rukwa rift. Frontiers in Earth Science, 9, p.707869.

Kolawole, F., Vick, T., Atekwana, E.A., Laó-Dávila, D.A., Costa, A.G., and Carpenter, B.M. (2022). Strain Localization and Migration During the Pulsed Lateral Propagation of the Shire Rift Zone, East Africa. Tectonophysics, 839, 229499. Doi: 10.1016/j.tecto.2022.229499.

Kolawole, F., Xue, L. and Dulanya, Z., 2023. Rapid Versus Delayed Linkage and Coalescence of Propagating Rift Tips. Authorea Preprints, 10.22541/essoar.168167202.29986035/v1.

Kranz, R. L. (1979). Crack-crack and crack-pore interactions in stressed granite. International Journal of Rock Mechanics and Mining Sciences and Geomechanics Abstracts, 16(1), 37–47.

Lavayssière, A., Drooff, C., Ebinger, C. J., Gallacher, R., Illsley-Kemp, F., Oliva, S. J., and Keir, D. (2019). Depth Extent and Kinematics of Faulting in the Southern Tanganyika Rift, Africa. Tectonics, 38, 842-862.

Lemna, O. S., Stephenson, R., and Cornwell, D. G. (2019). The Role of Pre-existing Precambrian Structures in the Development of Rukwa Rift Basin, Southwest Tanzania. J. Afr. Earth Sci. 150, 607–625. doi:10.1016/j.jafrearsci.2018.09.015.

Le Pourhiet, L., Chamot-Rooke, N., Delescluse, M., May, D.A., Watremez, L. and Pubellier, M., 2018. Continental break-up of the South China Sea stalled by far-field compression. Nature Geoscience, 11(8), pp.605-609.

Molnar, N.E., Cruden, A.R. and Betts, P.G., 2019. Interactions between propagating rifts and linear weaknesses in the lower crust. Geosphere, 15(5), pp.1617-1640.

Morley, C. K., Cunningham, S. M., Harper, R. M., and Wescott, W. A. (1992). Geology and Geophysics of the Rukwa Rift, East Africa. Tectonics 11 (1), 69–81. doi:10.1029/91tc02102.

Morley, C. K., Wescott, W. A., Harper, R. M., and Cunningham, S. M. (1999). Geology and Geophysics of the Rukwa Rift. Geoscience of Rift Systems-Evolution of East Africa. AAPG Stud. Geology. 44, 91–110.

Muirhead, J. D., Wright, L. J., and Scholz, C. A. (2019). Rift evolution in regions of low magma input in East Africa. Earth and Planetary Science Letters, 506, 332–346.

Mulaya, E., Gluyas, J., McCaffrey, K., Phillips, T. and Ballentine, C. (2022). Structural geometry and evolution of the Rukwa Rift Basin, Tanzania: Implications for helium potential. Basin Research 34, 938-960.

Nelson, R.A., Patton, T.L. and Morley, C.K., 1992. Rift-segment interaction and its relation to hydrocarbon exploration in continental rift systems. AAPG bulletin, 76(8), pp.1153-1169.

Neuharth, D., Brune, S., Glerum, A., Heine, C. and Welford, J.K., 2021. Formation of continental microplates through rift linkage: Numerical modeling and its application to the Flemish Cap and Sao Paulo Plateau. Geochemistry, Geophysics, Geosystems, 22(4), p.e2020GC009615.

Njinju, E.A., Atekwana, E.A., Stamps, D.S., Abdelsalam, M.G., Atekwana, E.A., Mickus, K.L., Fishwick, S., Kolawole, F., Rajaonarison, T.A. and Nyalugwe, V.N., 2019. Lithospheric structure of the Malawi Rift: Implications for magma-poor rifting processes. Tectonics, 38(11), pp.3835-3853.

Nunn, J.A., 1985. State of stress in the northern Gulf Coast. Geology, 13(6), pp.429-432.

Olson, J.E., 2004. Predicting fracture swarms—The influence of subcritical crack growth and the crack-tip process zone on joint spacing in rock. Geological Society, London, Special Publications, 231(1), pp.73-88.

Pérez-Gussinyé, M., Collier, J.S., Armitage, J.J., Hopper, J.R., Sun, Z. and Ranero, C.R., 2023. Towards a process-based understanding of rifted continental margins. Nature Reviews Earth & Environment, 4(3), pp.166-184.

Roberts, E. M., Stevens, N. J., O'Connor, P. M., Dirks, P. H. G. M., Gottfried, M. D., Clyde, W. C., Armstrong, R. A., Kemp, A. I. S., and Hemming, S. (2012). Initiation of the western branch of the East African Rift coeval with the eastern branch. Nature Geoscience, 5(4), 289–294. https://doi.org/10.1038/ngeo1432.

Shaban, S., Scholz, C.A., Kolawole, F. (2023). The Deep Basin and Underlying Basement Structure of the Tanganyika Rift. Tectonics, 42, e2022TC007726.

Stamps, D. S., Calais, E., Saria, E., Hartnady, C., Nocquet, J. M., Ebinger, C. J., and Fernandes, R. M. (2008). A kinematic model for the East African Rift. Geophysical Research Letters, 35(5).

Stein, S., Sleep, N.H., Geller, R.J., Wang, S.C. and Kroeger, G.C., 1979. Earthquakes along the passive margin of eastern Canada. Geophysical Research Letters, 6(7), pp.537-540.

Stevens, V.L., Sloan, R.A., Chindandali, P.R., Wedmore, L.N., Salomon, G.W., Muir, R.A., 2021. The entire crust can be seismogenic: evidence from Southern Malawi. Tectonics 40 (6). https://doi.org/10.1029/2020TC006654 e2020TC006654.

Tiercelin, J.J., Pflumio, C., Castrec, M., Boulégue, J., Gente, P., Rolet, J., Coussement, C., Stetter, K.O., Huber, R., Buku, S. and Mifundu, W., 1993. Hydrothermal vents in Lake Tanganyika, East African, Rift system. Geology, 21(6), pp.499-502.

Van Herwaarden, D., Thrastarson, S., Halpa, V., Afanasiev, M., Trampert, J., and Fichtner, A. (2022). Full-Waveform Tomography of the African Plate Using Dynamic Mini-Batches. Journal of Geophysical Research: Solid Earth, 126, 1-22.

Van Wijk, J.K., Blackman, D.K., 2005. Dynamics of continental rift propagation: the endmember modes. Earth Planet. Sci. Lett. 229 (3–4), 247–258.

Veatch, A. C. (1935). Evolution of the Congo Basin. GSA Memoir 3.

Versfelt, J., and Rosendahl, B. (1989). Relationship between pre-rift structure and rift architecture in Lakes Tanganyika and Malawi, East Africa. Nature, 337, 354–357.

Vidale, J. E. (1990). Finite-difference calculation of traveltimes in three dimensions. Geophysics, 55(5), 521-526.

Wessel, P., Luis, J. F., Uieda, L., Scharroo, R., Wobbe, F., Smith, W. H. F., and Tian, D. (2019). The generic mapping tools version 6. Geochemistry, Geophysics, Geosystems, 20, 1-20. https://doi.org/10.1029/2019gc008515

Yang, Z., and Chen, W. P. (2010). Earthquakes along the East African Rift System: A multiscale, system-wide perspective. Journal of Geophysical Research, 115, B12309. https://doi.org/10.1029/2009JB006779

Zheng, W., Oliva, S.J., Ebinger, C. and Pritchard, M.E., 2020. Aseismic deformation during the 2014 M w 5.2 Karonga earthquake, Malawi, from satellite interferometry and earthquake source mechanisms. Geophysical Research Letters, 47(22), p.e2020GL090930.

Zwaan, F., and Schreurs, G. (2020). Rift segment interaction in orthogonal and rotational extension experiments: Implications for the large-scale development of rift systems. Journal of Structural Geology, 140, 104119. https://doi.org/10.1016/j.jsg.2020.104119

Zwaan, F., Schreurs, G., Naliboff, J., and Buiter, S. J. (2016). Insights into the effects of oblique extension on continental rift interaction from 3D analogue and numerical models. Tectonophysics, 693, 239–260. https://doi.org/10.1016/j.tecto.2016.02.036